Department
of
APPLIED MATHEMATICS

Numerical studies of the current response at Ormen Lange to a travellling storm.

by

Frode Vikebø[1], Jarle Berntsen[1] and Gunnar Furnes[2]

Report no. 162 December 2001

UNIVERSITY OF BERGEN
Bergen, Norway

Department of Mathematics
University of Bergen
5008 Bergen
Norway

ISSN 0084-778X

Numerical studies of the current response at Ormen Lange to a travelling storm.

by

Frode Vikebø[1], Jarle Berntsen[1] and Gunnar Furnes[2]

[1]*Mathematical Institute, University of Bergen.*
[2]*Norsk Hydro, Research Center, Sandsli, Norway.*

Report no. 162

December 2001

Numerical studies of the current response at Ormen Lange to a travelling storm

Frode Vikebø[1], Jarle Berntsen[1] and Gunnar Furnes[2]

[1] *Mathematical Institute, University of Bergen, Norway.*

[2] *Norsk Hydro, Research Center, Sandsli, Norway.*

December 8, 2001

Abstract

An ongoing data acquisition program at Ormen Lange (OL), an offshore gas field located in the Storegga region off mid-Norway at depths from approximately 800 to 1100m, has identified several events in which the currents close to the sea bed exhibit a short peak value in their speed along with a peak in temperature. This may cause a significant loading on near sea bed installations such as pipelines. It is therefore essential to understand the generation mechanisms behind these events and to investigate the possibility of forecasting them.

Mean temporal circulation at OL is strongly dominated by the Norwegian Atlantic Current. Tidal effects are weak. The extreme events are driven by strong pressure gradients. That is, strong atmospheric low pressures and/or internal pressure fronts between warmer Atlantic Water (AW) and colder Norwegian Sea Water (NSW). Along the shelf slope at OL we may get steepening of the iso surfaces of density, separating AW and NSW, due to strong Ekman veering during storms or approaching internal density fronts. During such events the density surfaces tend to undershoot their equilibrium level, and as the forcing weaken, the suppressed water may run up along the shelf slope. In this run up phase, peak values in the velocities are often found. Since the atmospheric forcing is a major forcing mechanism behind the observed events, we have studied the sensitivity of near bottom velocities at OL to the pathway of the low pressure disturbances and the strength and the radius of them.

1 Introduction

Ormen Lange is an offshore gas field located in the Storegga region off mid-Norway in water depths from approximately 800 to 1100m. The field, presently being considered for development under the leadership of Norsk Hydro, is located in the core of the Storegga slide that left an almost 300m long headwall at the shelf break. Extracting and transporting gas from the reservoir includes seabed pipeline tracks which makes it essential to know the maximum velocities in the region. This report will focus on near seabed velocities, as as possible pipelines are to be located there.

The water masses in the region may be divided into four different layers classified by their origin, where the depth of the interfaces may vary both in time and space (Hopkins 1991):

- Norwegian Coastal Water (NCW) on shelf with salinity 32 - 35 p.s.u. and temperature 2 - 13°C due to inflow from the Baltic and runoff from Norwegian rivers,
- Norwegian Atlantic Current (NAC) off shelf with salinity above 35.0 p.s.u. and temperature above 2°C,
- Norwegian Sea Artic Intermediate Water (NSAIW) with salinity below 34.9 p.s.u. and temperature between -0.5 and 0.5°C,
- Norwegian Sea Deep Water (NSDW) with salinity 34.91 p.s.u. and temperature less than -0.5°C.

The upper layer of warm and salt NAW interface with the cold and fresher NSAIW at around 400 to 600m and the interface rises towards the west. The NSDW is located below 800 m. The different water masses give rise to strong density fronts (horizontally and vertically) along which a wide range of wave and meandering phenomena may occur. The water masses of the upper layer are subject to significant variations due to atmospheric forcing and has a significant directional variability and maximum velocities above $1 ms^{-1}$. The water masses below are clearly more stable and mean direction aligns with large scale bottom topography and have an average speed of 20 to $30 cms^{-1}$. Water masses close to the seabed are more directional unstable than the water masses above, and have lower average velocities. However, intermittent events of short term peaks in velocities and abrupt changes in temperatures are observed close to the seabed and described/discussed in Eliassen et al. (2000), Vikebø et al. (2001) and Mathisen et al. (2000). Also, Eliassen & Berntsen (2000) and Engedahl & Røed (1999) have studied local dynamics using ocean models.

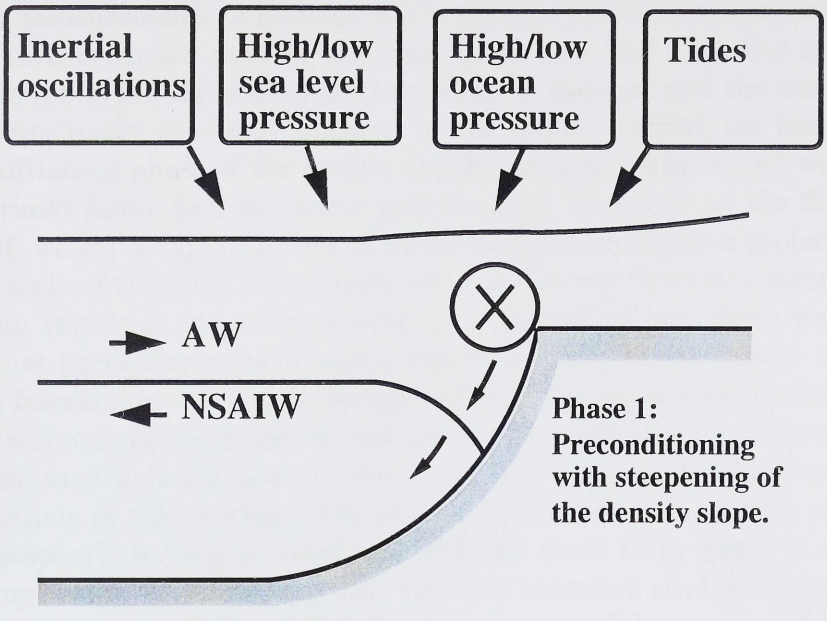

Figure 1: *A plausible model explaining the current response at Ormen Lange to a passing low pressure disturbances in the Nordic Seas.*

Cyclonic wind around a storm center induces Ekman transport in the upper layer away from the low pressure center with a subsequent lowering of the surface, though this is partly compensated by an elevation of the surface due to a lower atmospheric pressure (a change of 1 hPa corresponds approximately to a change in sea level of 1 cm (Gjevik 1991)). A resulting upward Ekman transport, known as Ekman-pumping, causes a transport towards the atmospheric low pressure center in the deeper layer of the water column. Low pressure disturbances normally follow trajectories entering the area of the Nordic Seas around Iceland and then turns north-east towards Svalbard and the Barents Sea. This causes south-westerly winds along the coast of Norway, with surface elevation towards the coast. A subsequent strengthening of the Atlantic inflow along the Norwegian coast cause penetration of the NAC to greater depth. Increased Ekman veering along the seabed enhance this vertical extension of the flow. The overall result of passing low pressure disturbances in the Nordic Seas will be a steepening of the iso surfaces of density towards the shelf slope at Ormen Lange, Figure 1. This down welling increases the near seabed temperature, but as the thermocline is located around 400 to 600m depth, the highest temperature change will be located just below the thermocline.

Prognostic variables at Ormen Lange and the shelf slope above from a numerical model of the Nordic Seas forced by a travelling storm was compared

with measurements in Eliassen et al. (2000). Values from the simulation and the measurements were of the same order and had a similar spatial distribution, but the rapidity of the temperature changes and the associated high velocity peaks were not captured by the model. During the build up or pre conditioning phase of the events, the dominating features and waves may be captured farely well by coarse grid models. However, as the flow turns on shelf, we get a superposition of waves on a range of scales probably down to the scale of the local topography and the bottom boundary layer. The maximum velocities at a given locality will depend on how these waves interact at that particular point in space and time. We can not expect to reproduce this interaction exactly, especially not with the present resolution. However, the response of the model on the near bottom velocities to different low pressures, may indicate how the time and space averaged velocities develop as functions of this forcing. The results of Vikebø et al. (2001) indicate that atmospheric forcing is correlated with the short term peaks in velocity and abrupt changes in temperature. We have therefore studied the sensitivity of the velocities at Ormen Lange to the pathway of the storm and the strength and radius of the low pressure disturbance. In reality, the strength of the peak events will depend on the interference between smaller scale phenomena at the particular locations.

2 Model setup

A basin scale model was set up, with climatological initial and boundary conditions, forced by idealised storms passing by Ormen Lange in the adjacent Nordic Seas.

Location	OL1	OL2	OL3	OL4	OL5
Depth	257.0	499.0	835.9	1120.1	764.4

Table 1: *The depth at station OL1 to OL5 as indicated in Figure 2. Depth in meter.*

The system of equations and the numerical σ-coordinate ocean model are described by Berntsen (2000). The equations are the continuity equation for an incompressible fluid, the Reynolds averaged momentum equations horizontally, conservation equations for temperature and salinity and the

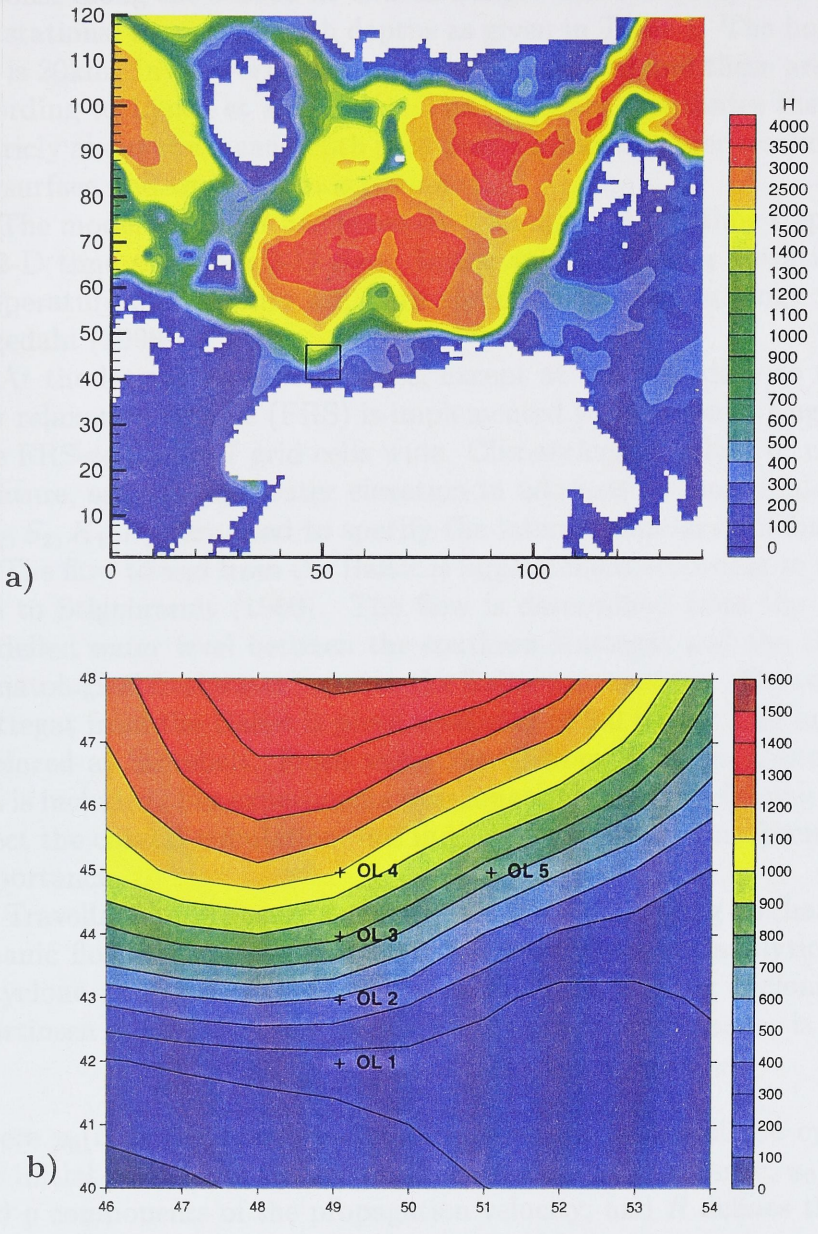

Figure 2: *a) The model area with with Ormen Lange outlined. b) The Ormen Lange area with the locations OL1 to OL5 with depths as indicated in Table 1. Unit of axis in grid coordinates of 20km.*

UNESCO-equation of state, see Gill (1982). The model assumes Boussinesq and hydrostatic approximation.

The model area covers the Norwegian Sea basin, Figure 2a, with focus on response along the seabed at Ormen Lange. The local response is studied at five stations, Figure 2b, with depths as given in Table 1. The horizontal grid size is 20km. In the vertical 30 σ-layers are applied and these are distributed according to Lynch et al. (1995). Their formula distributes the layers symmetricly about the mean depth such that a gradually finer resolution towards the surface and the bottom is obtained.

The model is run for 240 hours with an internal 3-D time step of 360s and 30 2-D time steps per 3-D step. Initial values of water elevation, velocity, temperature and salinity are from the diagnostic climatology described in Engedahl (1998).

At the lateral open boundaries, except at the boundary to the Baltic, a flow relaxation scheme (FRS) is implemented (Martinsen & Engedahl 1987). The FRS-zones are 7 grid cells wide. Climatological values of velocity, temperature, salinity and water elevation in addition to four tidal constituents (M_2, S_2, K_1, N_2) are used to specify the lateral boundary conditions.

The flow to and from the Baltic is implemented according to an algorithm due to Stigebrandt (1980). The flow is determined from the difference in modelled water level between the southern Kattegat and the Baltic, taking climatological freshwater input to the Baltic into account. The water entering Kattegat from the Baltic is given a salinity of 8.0 p.s.u.. The inflow/outflow is placed at Storebelt. Fresh water runoff from 27 rivers around the North Sea is included. For experiments over longer periods this forcing will strongly affect the coastal circulation, but in the present study this forcing has minor importance.

Travelling low pressure systems are important driving mechanisms for the oceanic flow. Martinsen et al. (1979) constructed an analytical model for a cyclone and studied barotropic effects of the moving cyclone. Following Martinsen et al. (1979) the atmospheric pressure disturbance is described by

$$p(x,y,t) = p_0(t)e^{\{-[(x-x_0-u_0t)^2+(y-y_0-v_0t)^2]/R^2\}} \quad , \tag{1}$$

where $p_0(t)$ is the pressure disturbance at the center of the cyclone; x_0, y_0 the initial position of the center of the pressure disturbance; u_0, v_0 are the x and y components of the propagation velocity; and R defines the horizontal extent of the pressure disturbance. Wind velocity components u_g and v_g in the x and y directions, respectively, are computed from the atmospheric pressure gradients as

$$u_g = -\frac{0.7}{f\rho_a}\frac{\partial p}{\partial y} \quad , \tag{2}$$

$$v_g = \frac{0.7}{f\rho_a}\frac{\partial p}{\partial x} \quad , \tag{3}$$

where f is the Coriolis parameter and ρ_a the density of the air (1.3 kg m^{-3}).

The wind stress is computed from the wind velocity components as

$$\tau_x = \rho_a c_D (u_g^2 + v_g^2)^{1/2} u_g \quad , \tag{4}$$

$$\tau_y = \rho_a c_D (u_g^2 + v_g^2)^{1/2} v_g \quad , \tag{5}$$

where c_D is the drag coefficient. In our experiments c_D is chosen to be 3×10^{-3} following Martinsen et al. (1979).

It could be conjectured that the rapid changes in near bottom temperature and velocities at Ormen Lange at midnight on the 16 November 1996, Figure 3, were related to a low pressure system entering the Norwegian Sea basin close to Greenland on 14 November 1996, Figure 4. The low pressure system was moving with a speed of approximately 10ms^{-1} towards the Barents Sea and had a minimum value of 952hPa (1hPa=100Pa=100Nm^{-1}) south of Island at midnight on the 15 November. Based on the weather maps from this period, the horizontal extent of the low pressure system is estimated to be about 1000km. In order to study the numerical response of this low pressure on the flow at Ormen Lange the model is run with parameters as given for Run_track1 in Table 2. The sensitivity of the velocities at Ormen Lange to the pathway of the storm and the strength and the radius of the low pressure disturbance is also studied by varying one parameter at a time.

The model is first run 24 hours with $p_0(t) = 0$. The low pressure system is then started at position (x_0, y_0) given in grid coordinates in Table 2 and $p_0(t)$ is increased linearly over the next 12 hours to the values given in the table and held constant for the remaining simulation period. In the grid coordinate system x and y components of the propagation velocities are u_0 = 8.59ms^{-1} and v_0 = -4.81ms^{-1} respectively in all experiments.

In the experiments Run_track1 to Run_track4 the shortest distances between the center of the low pressures and Ormen Lange are 1000km, 667km, 333km and 0km respectively. The radius of the circle of maximum wind speed is 707km ($R/\sqrt{2}$) for R = 1000km. The strongest response on the currents at Ormen Lange was found for Run_track2 where we have maximum wind speed approximately along the shelf slope. The sensitivity to the low pressure disturbance, p_0, is therefore studied for the pathway used for Run_track2. In the studies where R is gradually decreased, the pathways of the storms are also based on the pathway given for Run_track2. The starting points (x_0, y_0) are, however, adjusted such that the position of maximum wind speed along the shelf slope at Ormen Lange is kept unchanged.

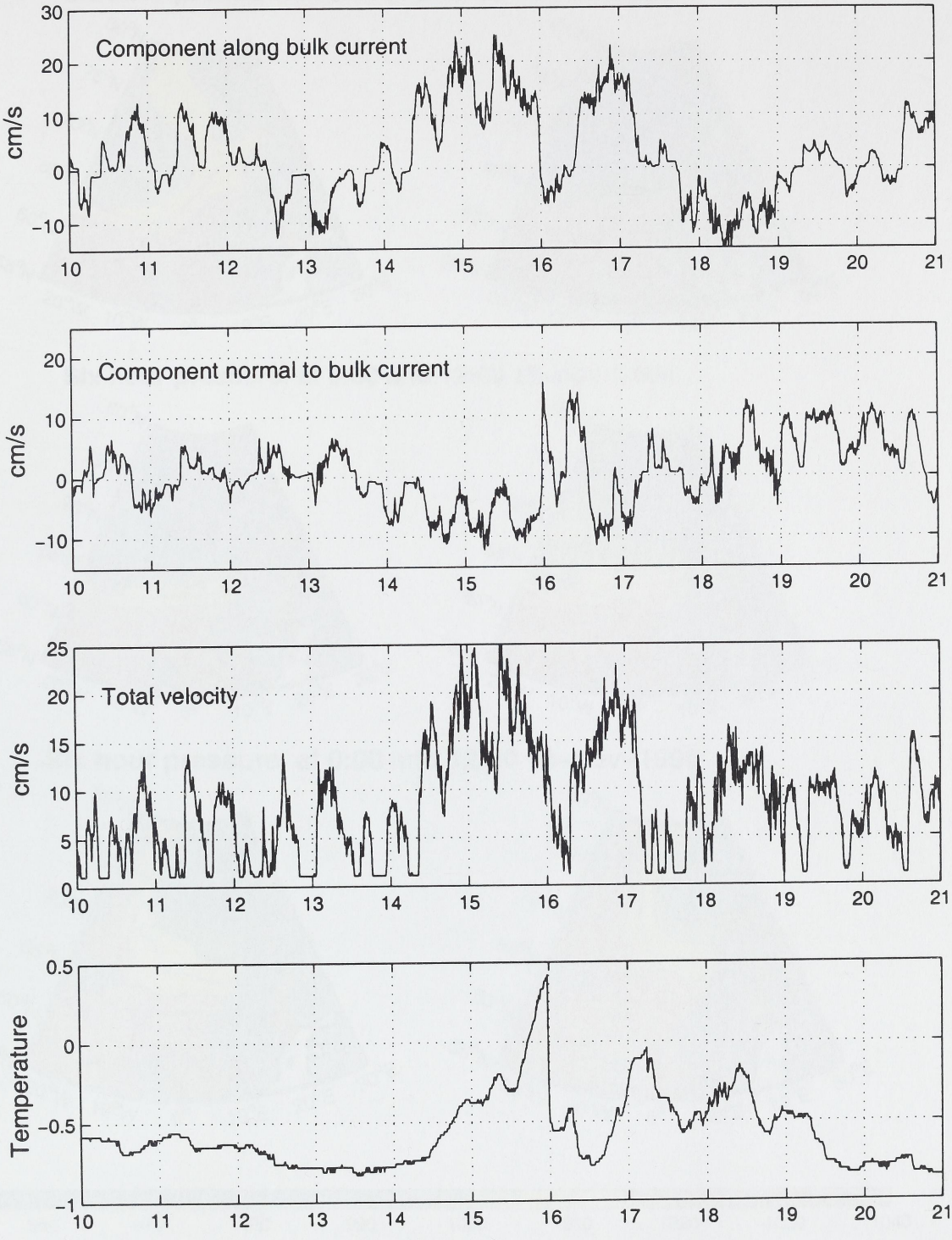

Figure 3: *Currents and temperature at OL2 764 m, 5m above seabed, November 10 until 21 1996.*

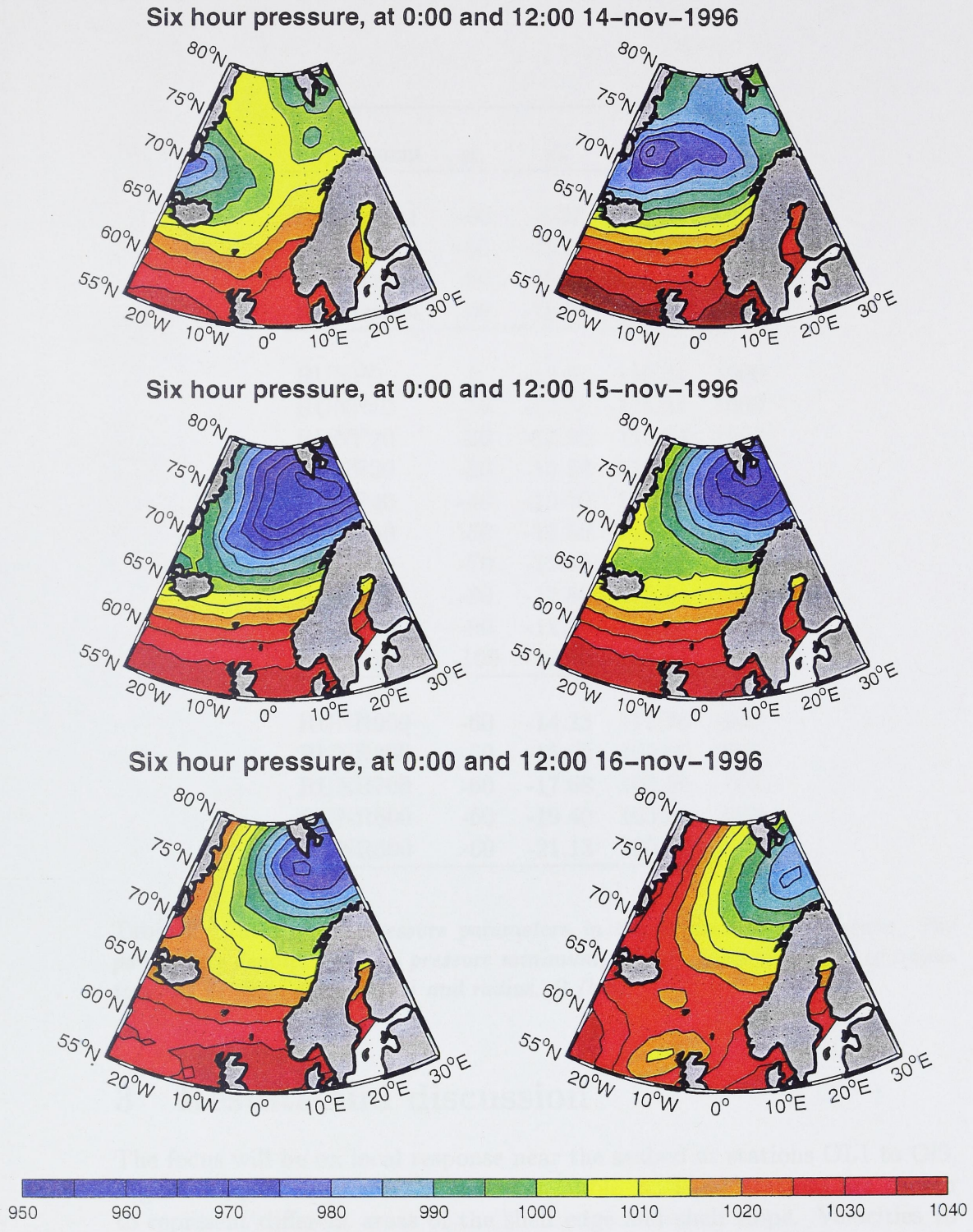

Figure 4: *Sea level pressure from the NMI hindcast archive at 0:00 and 12:00 h November 14, 15 and 16 1996.*

Experiment	p_0	x_0	y_0	R
Run_track1	-60	-4.37	130.38	1000
Run_track2	-60	-12.50	115.84	1000
Run_track3	-60	-20.63	101.30	1000
Run_track4	-60	-28.76	86.76	1000
RUNP0	0	-12.50	115.84	1000
RUNP10	-10	-12.50	115.84	1000
RUNP20	-20	-12.50	115.84	1000
RUNP30	-30	-12.50	115.84	1000
RUNP40	-40	-12.50	115.84	1000
RUNP50	-50	-12.50	115.84	1000
RUNP70	-70	-12.50	115.84	1000
RUNP80	-80	-12.50	115.84	1000
RUNP90	-90	-12.50	115.84	1000
RUNP100	-100	-12.50	115.84	1000
RUNR900	-60	-14.23	112.76	900
RUNR800	-60	-15.95	109.67	800
RUNR700	-60	-17.68	106.59	700
RUNR600	-60	-19.40	103.50	600
RUNR500	-60	-21.13	100.42	500

Table 2: *Table of low pressure parameters in the numerical experiments. The parameters denote: sea level pressure minimum, p_0 (hPa), starting point of trajectory, x_0, y_0 (grid coordinates) and radius, R (km).*

3 Results and discussion

The focus will be on local response near the seabed at stations OL1 to Ol5, Figure 2b, with depths as indicated in Table 1. These stations are chosen to represent different areas of the shelf edge and shelf slope. Velocities 10 and 50m above seabed are presented and the results will be discussed in the following sections.

Maximum velocities at OL are typically seen during maximum wind speed. As the center of the low pressure leaves the OL area, a transient period of interference between two dominating frequencies occurs. Barotrope

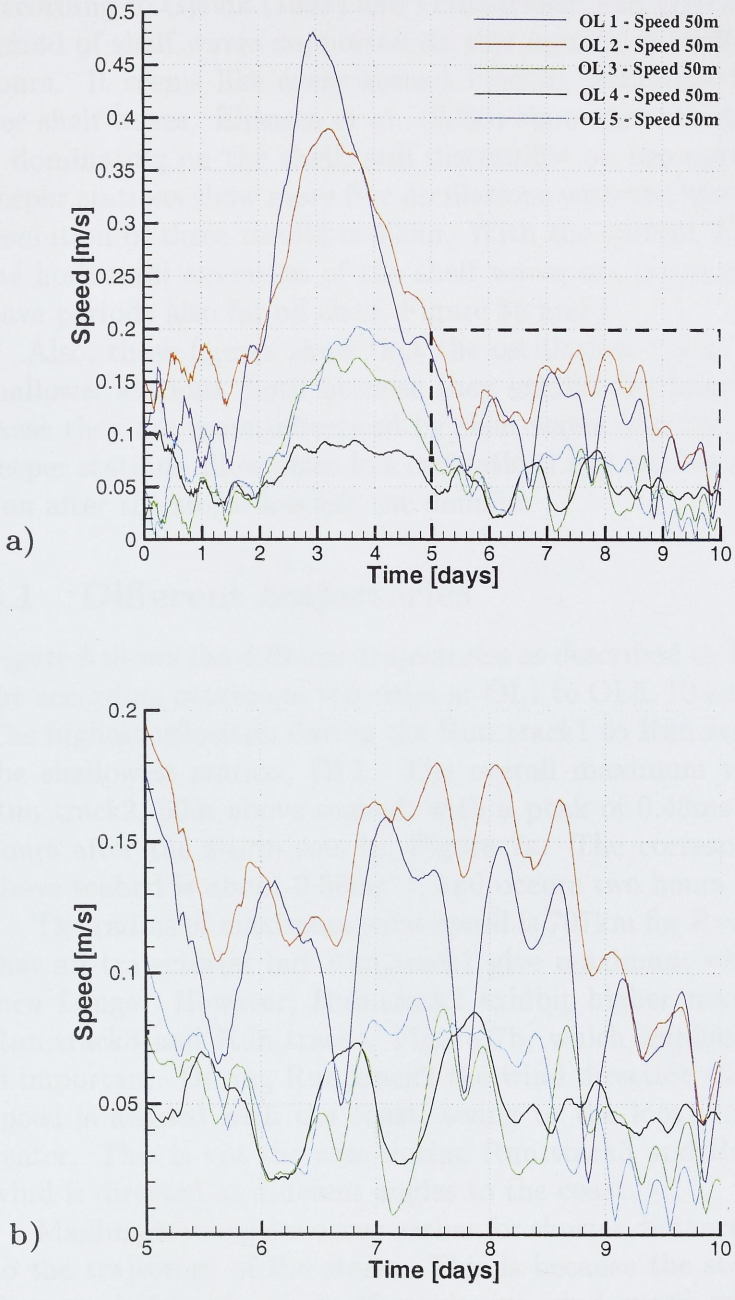

Figure 5: *a) Total velocity 50m above seabed at OL1 to OL5 during Run_track2. b) Same as above but focusing on the last five days as indicated by the dashed box in a.*

shelf waves with period of about 24 hours and inertial oscillations with period of about 13.4 hours. From around day 8 to 9 only inertial oscillations remains. According to Gjevik (1991) and Ommundsen and Gjevik (2000) the shortest period of shelf waves supported on this particular shelf is approximately 20 hours. It seems like every second inertial oscillation feed energy into the free shelf waves. Eliassen et al. (2000) show that the double inertial period is dominating on the shelf, still discernible on the upper shelf slope, while deeper stations show more free oscillations with the inertial period. The grid resolution of these results is 400m. With the current 20 km grid resolution, the horizontal extension of the shelf waves are misrepresented, giving shelf wave periods also far off shelf, Figure 5a and b.

Also, these figures show that the oscillations decay more quickly at the shallower stations, both because they exhibit the largest velocities and because they are more influenced by shelf waves and the Atlantic inflow. The deeper stations allow more free oscillations and exhibit less amplitude reduction after the storm has left the domain.

3.1 Different trajectories

Figure 6 shows the different trajectories as described in Table 2. Table 3 gives the according maximum velocities at OL1 to OL5, 10 and 50m above seabed. The highest velocities during the Run_track1 to Run_track4 are all found on the shallowest station, OL1. The overall maximum velocity occur during Run_track2, 50m above seabed, with a peak of $0.48 ms^{-1}$ after 73 hours, 49 hours after the storm sets in, Figure 7a. The corresponding velocity 10m above seabed is about $0.38 ms^{-1}$, and occurs two hours later.

The radius of maximum wind-speed is 707km for R=1000km. This means that all trajectories but Run_track1 give maximum wind speeds above Ormen Lange. However, Run_track2 exhibit higher maximum velocity than Run_track3 and Run_track4, Figure 7b, which implies that wind direction is important. During Run_track2 the wind direction during maximum wind speed is aligned with the coast, owing to the location of the low pressure center. This is not the case during Run_track3 and Run_track4, where the wind is directed at different angles to the coast.

Maximum velocities occur earlier for shorter distances from Ormen Lange to the trajectory of the storm. This is because the storm travels a shorter distance before the circle of maximum wind speed reaches Ormen Lange. Since the circle of maximum wind speed does not reach Ormen Lange at all during Run_track1, so the maximum wind speed occurs as the direction from Ormen Lange to the low pressure center is normal to the storm trajectory.

The earliest peaks have also the largest secondary peak, both relative to

the primary peak itself, but also in comparison with the other trajectories. The reason might be that when the shortest distance from Ormen Lange to the trajectory of the storm is less then the radius of the circle of maximum wind speed, there are two occasions where the circle crosses Ormen Lange. Simple geometrical considerations show that for Run_track2, this occurs after 2.8 days and 3.4 days. This is clearly too close to observe two separate peaks in current velocities close to the seabed. For Run_track3 the times are 2.4 days and 3.8 days, and for Run_track4 the times are 2.3 days and 4.0 days. Only Run_track4 show any sign of a split primary peak, indicating that only Run_track4 gives enough time between the two peaks of wind for this to be seen on the time series of current velocity.

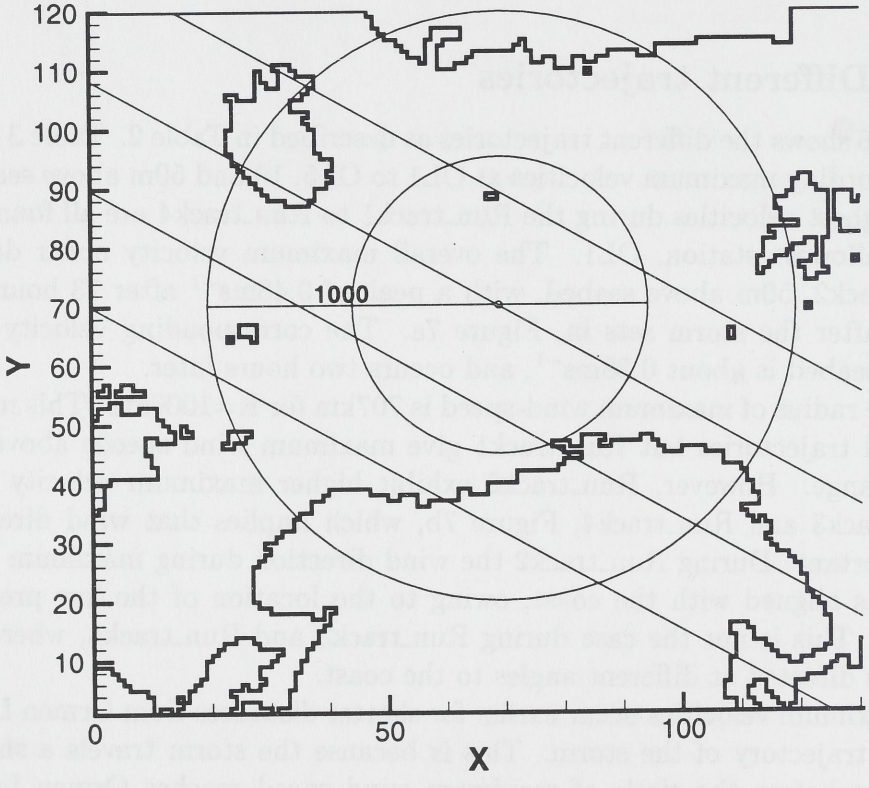

Figure 6: *The different trajectories during Run_track1 to Run_track4 as described in Table 2, and the extension of the low pressure disturbances for* $R = 1000km$ *and* $R = 500km$*, shown for Run_track2. Unit of axis in grid coordinates of 20km.*

a)

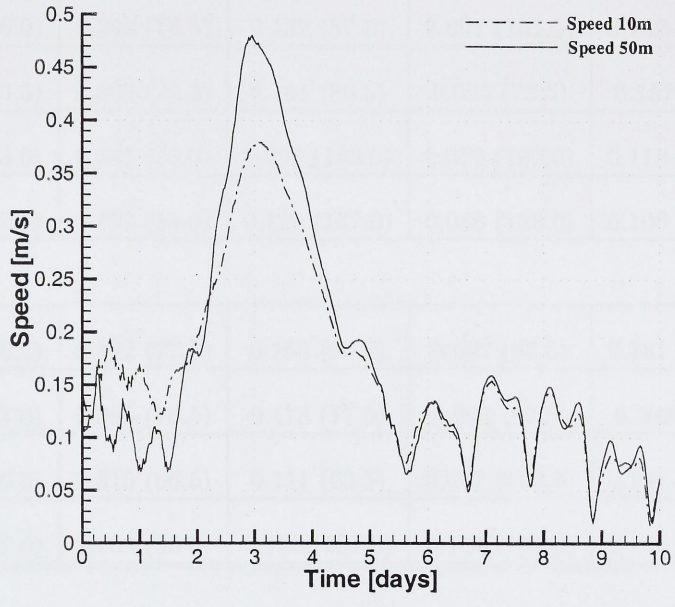

b)

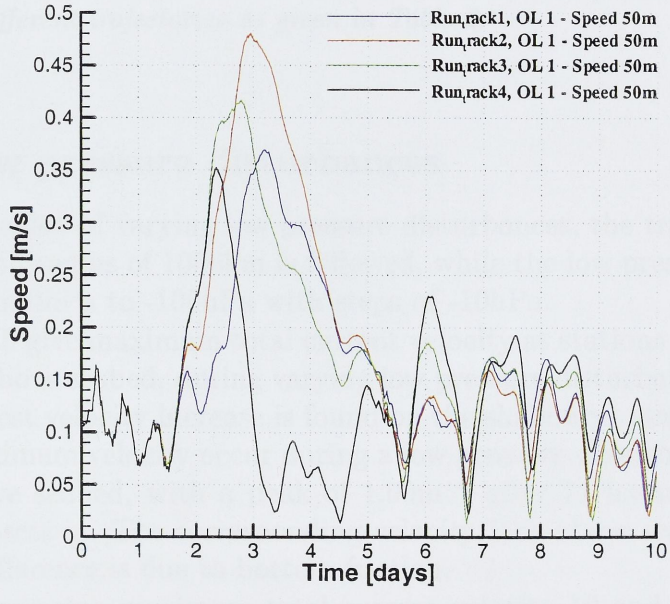

Figure 7: *a) Total velocity 10 and 50m above seabed at OL1 during Run_track2. b) Total velocity 50m above seabed at OL1 during Run_track1 to Run_track4.*

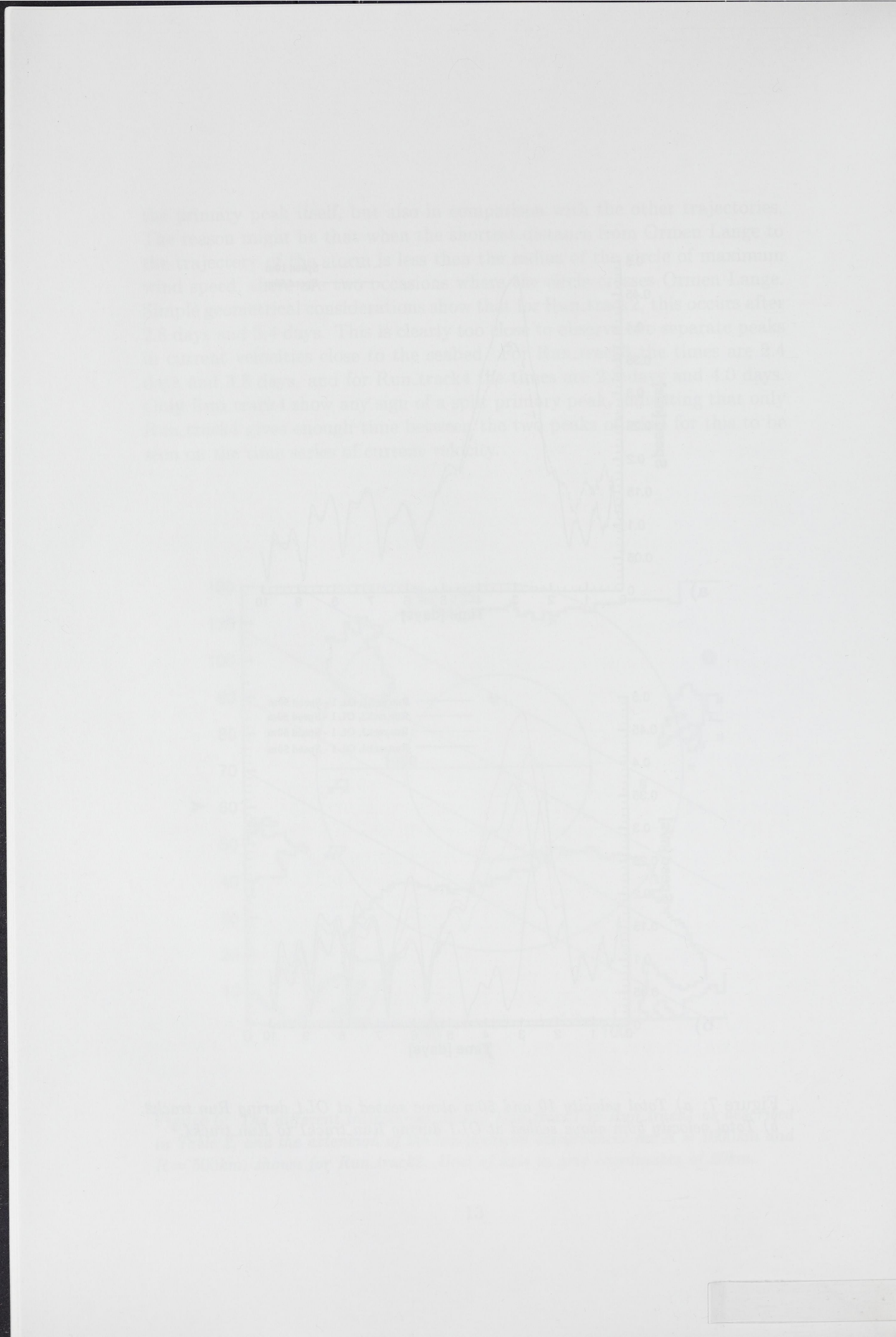

10 m	OL1	OL2	OL3	OL4	OL5
Run_track1	0.303 (76.0)	0.249 (78.5)	0.132 (87.5)	0.091 (101.5)	0.142 (106.5)
Run_track2	0.380 (73.5)	0.305 (76.5)	0.141 (86.5)	0.094 (73.5)	0.157 (88.0)
Run_track3	0.326 (63.0)	0.245 (66.0)	0.098 (182.0)	0.072 (189.0)	0.118 (106.5)
Run_track4	0.281 (57.5)	0.197 (55.0)	0.129 (157.0)	0.088 (138.0)	0.106 (150.0)
50 m					
Run_track1	0.369 (76.5)	0.322 (77.0)	0.168 (90.0)	0.092 (87.5)	0.181 (104.0)
Run_track2	0.480 (71.0)	0.389 (76.5)	0.173 (77.0)	0.094 (87.0)	0.202 (89.0)
Run_track3	0.416 (66.5)	0.315 (66.5)	0.111 (63.5)	0.077 (190.0)	0.147 (106.0)
Run_track4	0.352 (57.0)	0.253 (55.0)	0.133 (157.0)	0.104 (138.0)	0.108 (151.0)

Table 3: *Maximum velocity (ms^{-1}) at OL1 to OL5, and time of occurance (h) after simulation start in parenthesis, 10 and 50m above seabed. Run_track1 to Run_track4 describes different trajectories as given in Table 2.*

3.2 Varying low pressure disturbances

In order to study the effect of varying low pressure disturbances, the trajectory of Run_track2 with radius of 1000km is followed, while the low pressure disturbance range from 0hPa to -100hPa with steps of -10hPa.

Table 4 and Table 5 give maximum total current velocity at stations OL1 to OL5, 10 and 50m above seabed, during varying low pressure disturbances. As expected, the highest velocity increase is found on the shallowest station, OL1. The overall maximum velocity occur during a low pressure disturbance of -100hPa, 50m above seabed, with a peak of $1.00m^{-1}$ after 71 hours, 47 hours after the storm sets in. The corresponding velocity 10m above seabed is $0.79m^{-1}$ and the difference is due to bottom friction.

Figure 8 shows increasing maximum total current velocity 10 and 50m above seabed with increasing low pressure disturbance at OL1 to OL5. As expected a weak low pressure disturbance gives practically no increased current velocities close to the seabed at Ormen Lange. It takes at least a low pressure disturbance of about -20hPa to increase the current velocities, when

10 m	OL1	OL2	OL3	OL4	OL5
RunP0	0.152 (38.0)	0.109 (39.5)	0.042 (158.0)	0.053 (36.5)	0.050 (239.0)
RunP10	0.153 (38.0)	0.119 (74.5)	0.042 (158.0)	0.053 (36.5)	0.051 (239.0)
RunP20	0.168 (76.5)	0.138 (78.5)	0.045 (105.5)	0.053 (36.5)	0.056 (239.0)
RunP30	0.195 (74.5)	0.164 (74.5)	0.060 (87.5)	0.054 (36.5)	0.080 (107.5)
RunP40	0.240 (75.0)	0.198 (76.5)	0.085 (87.5)	0.062 (62.5)	0.101 (106.5)
RunP50	0.306 (73.5)	0.246 (76.5)	0.122 (87.0)	0.075 (63.5)	0.125 (88.5)
RunP60	0.380 (73.5)	0.305 (76.5)	0.141 (86.5)	0.095 (73.5)	0.157 (88.0)
RunP70	0.468 (73.5)	0.364 (76.5)	0.183 (85.5)	0.119 (84.5)	0.195 (85.5)
RunP80	0.564 (71.0)	0.437 (79.0)	0.223 (82.5)	0.148 (74.5)	0.239 (83.0)
RunP90	0.669 (71.0)	0.514 (79.0)	0.272 (82.5)	0.182 (86.0)	0.289 (83.0)
RunP100	0.789 (71.1)	0.603 (74.5)	0.334 (83.5)	0.223 (84.5)	0.341 (82.0)

Table 4: *Maximum velocity (ms^{-1}) at OL1 to OL5, and time of occurrence (h) after simulation start in parenthesis, 10m above seabed. $P = 0$ to$P = -100$ describes different low pressure disturbances ranging from 0 to -100hPa, with radius 1000km, following the trajectory of Run_track2, as described in Table 2.*

the radius of the low pressure disturbance is 1000km. Above this threshold the pressure clearly affects current velocities.

The deeper stations, OL3 to OL5 display a smaller change with increasing low pressure disturbance than the shallower stations, OL1 and OL2. Maximum values at OL3 and OL5, 50m (10m) above seabed, are about $0.42m^{-1}$ ($0.33m^{-1}$) and $0.43m^{-1}$ ($0.34m^{-1}$) respectively, while OL4 has a peak of $0.26m^{-1}$ ($0.22m^{-1}$) 50m (10m) above seabed.

Figure 9 show how the maximum current velocity 10 and 50m above seabed are delayed with depth. Although there are few stations, the figure suggests an almost linear connection between depth and time of peak current. Though the maximum current velocity occurs instantaneously at 250m depth as the maximum wind speed is located above, the maximum current velocity at 1100m depth is delayed with approximately 16 hours.

a)

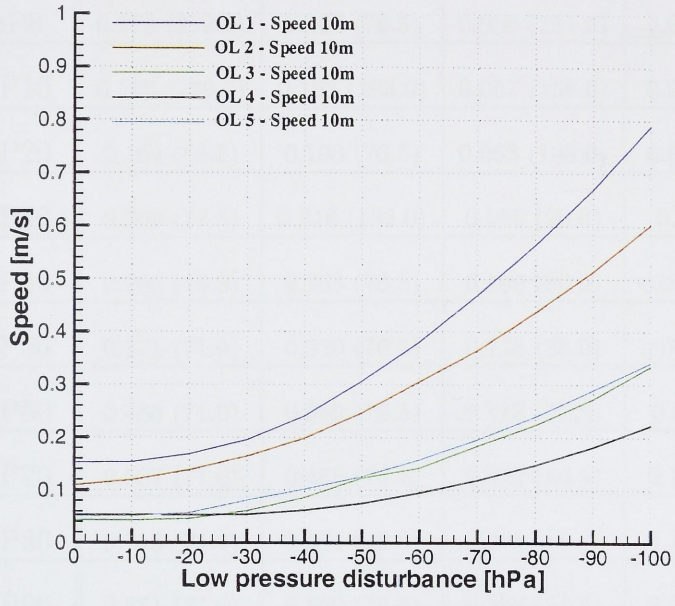

b)

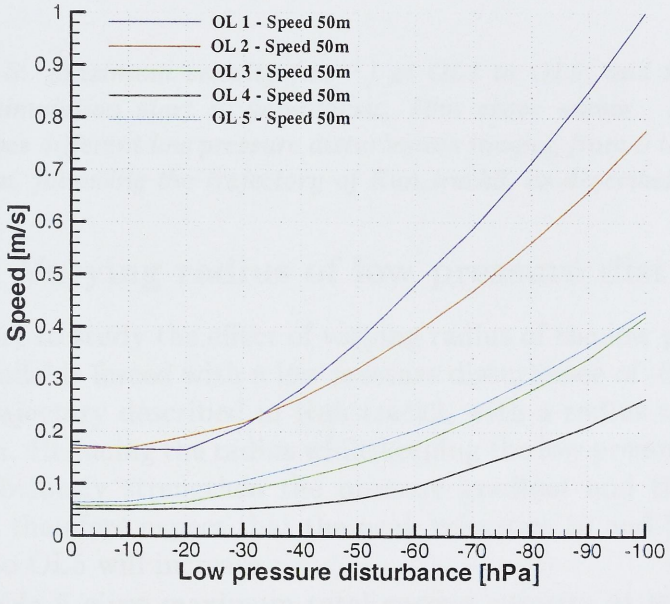

Figure 8: *a) Increasing maximum total current velocity 10m above seabed with increasing low pressure disturbance at OL1 to OL5. b) The same as the previous figure but 50m above seabed.*

50 m	OL1	OL2	OL3	OL4	OL5
RunP0	0.173 (219.5)	0.167 (76.5)	0.056 (131.5)	0.051 (37.0)	0.063 (239.5)
RunP10	0.166 (219.5)	0.168 (103.0)	0.057 (158.0)	0.051 (37.5)	0.065 (166.5)
RunP20	0.164 (69.5)	0.190 (76.5)	0.063 (105.0)	0.052 (37.5)	0.081 (106.5)
RunP30	0.209 (77.5)	0.216 (102.0)	0.085 (90.0)	0.05237.5)	0.105 (104.0)
RunP40	0.280 (76.5)	0.263 (76.5)	0.109 (90.0)	0.059 (189.0)	0.133 (104.0)
RunP50	0.371 (71.0)	0.320 (76.5)	0.138 (88.0)	0.072 (188.5)	0.166 (91.0)
RunP60	0.480 (71.0)	0.389 (76.5)	0.173 (77.0)	0.094 87.0)	0.202 (89.0)
RunP70	0.587 (71.0)	0.468 (76.5)	0.222 (86.5)	0.132 (84.5)	0.244 (89.5)
RunP80	0.713 (71.0)	0.561 (79.0)	0.278 (80.0)	0.169 (81.5)	0.300 (87.0)
RunP90	0.851 (71.0)	0.660 (78.5)	0.339 (84.5)	0.211 (84.5)	0.363 (78.0)
RunP100	1.004 (71.0)	0.777 (76.5)	0.420 (82.5)	0.264 (84.5)	0.431 (81.0)

Table 5: *Maximum velocity (ms^{-1}) at OL1 to OL5, and time of occurrence (h) after simulation start in parenthesis, 50m above seabed. $P = 0$ to $P = -100$ describes different low pressure disturbances ranging from 0 to -100hPa, with radius 1000km, following the trajectory of Run_track2, as described in Table 2.*

3.3 Varying radius of low pressure disturbances

In order to study the effect of varying radius of the low pressure disturbance, the model is forced with a low pressure disturbance of -60hPa, initially along the trajectory described in Run_track2, with a radius ranging from 1000 to 500km. Reducing the radius while keeping the low pressure disturbance fixed, will obviously strengthen the pressure gradient and thus the winds. One would therefore expect that the peak velocities 10 and 50m above seabed at OL1 to OL5 will increase.

Table 6 gives maximum total current velocity at stations OL1 to OL5, 10 and 50m above seabed. The highest velocity increase is found on the shallowest station with a peak of $1.27 m^{-1}$, 50m above seabed, during a low pressure disturbance of -60hPa with radius of 500km. The corresponding velocity 10m above seabed is $0.99 m^{-1}$.

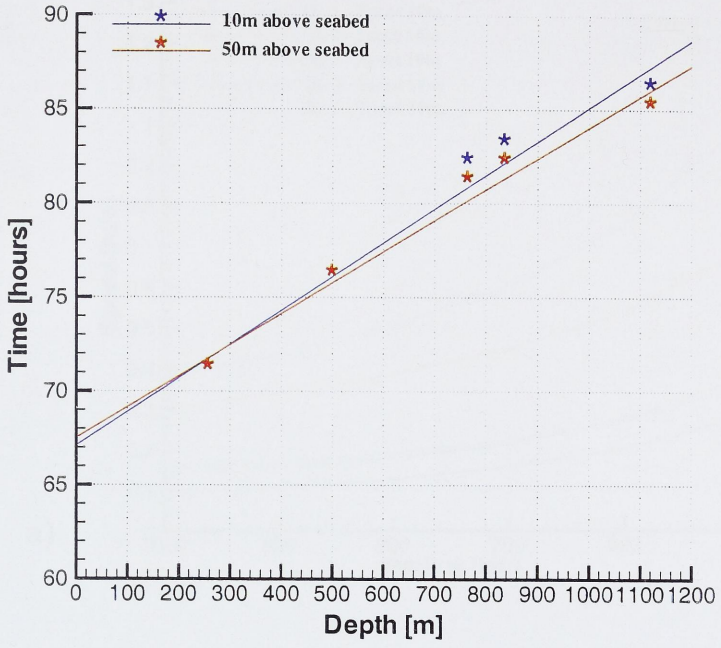

Figure 9: *Time of peak current velocity with depth along with a best fit linear regression line. The two shallowest points are common for both 10 and 50m above sea bed.*

Figures 10a and b show how the maximum current velocities increase with decreasing radius of the low pressure disturbance, 10 and 50m above seabed. The figures indicate a linear relationship between radius and velocities as the radius decreases to about 700km. Beyond this the increase tends to accelerate.

Increasing the low pressure strength has the same effect on the winds as reducing the radius, as the sea level pressure gradient is proportional to wind strength (Equation 2). Increasing the low pressure disturbance to -100hPa, holding the radius fixed at 1000km, is therefore comparable to reducing the radius of the disturbance to 600km, holding the disturbance fixed at -60hPa. This is reflected in Table 4, 5 and 6.

a)

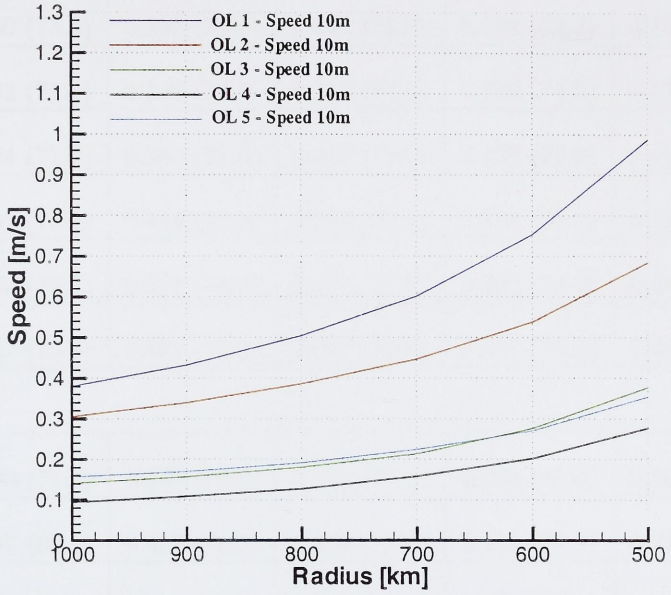

b)

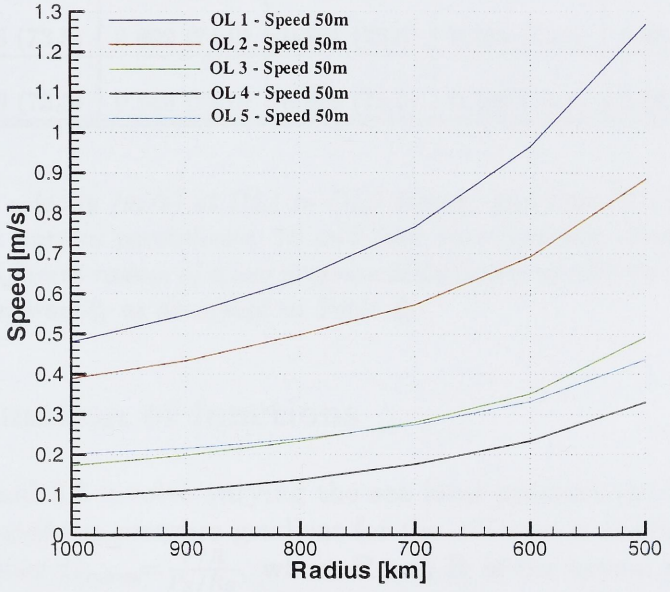

Figure 10: *a) Increasing maximum total current velocity 10m above seabed with radius of the low pressure disturbance at OL1 to OL5. b) The same as the previous figure but 50m above seabed.*

10 m	OL1	OL2	OL3	OL4	OL5
RunR1000	0.380 (73.5)	0.305 (76.5)	0.141 (86.5)	0.094 (73.5)	0.157 (88.0)
RunR900	0.432 (71.0)	0.339 (76.5)	0.157 (87.0)	0.109 (74.5)	0.170 (86.0)
RunR800	0.504 (71.0)	0.385 (77.5)	0.180 (75.0)	0.127 (73.5)	0.191 (81.5)
RunR700	0.601 (71.0)	0.446 (73.0)	0.213 (77.0)	0.158 (75.0)	0.224 (80.5)
RunR600	0.753 (73.5)	0.537 (74.0)	0.276 (77.0)	0.202 (74.5)	0.270 (80.0)
RunR500	0.987 (73.5)	0.684 (74.0)	0.377 (76.0)	0.277 (74.5)	0.354 (75.0)
50 m					
RunR1000	0.480 (71.0)	0.389 (76.5)	0.173 (77.0)	0.094 (87.0)	0.202 (89.0)
RunR900	0.547 (69.5)	0.433 (76.5)	0.198 (77.0)	0.110 (75.0)	0.215 (88.0)
RunR800	0.637 (71.0)	0.498 (76.5)	0.233 (77.0)	0.137 (75.5)	0.239 (80.5)
RunR700	0.766 (71.0)	0.572 (74.5)	0.280 (75.0)	0.176 (77.0)	0.274 (80.5)
RunR600	0.966 (73.5)	0.692 (74.0)	0.351 (73.5)	0.234 (75.5)	0.332 (78.5)
RunR500	1.269 (73.5)	0.885 (74.0)	0.492 (75.0)	0.330 (74.5)	0.436 (76.0)

Table 6: *Maximum velocity (m/s) at OL1 to OL5 during, and time of occurrence (h) after simulation start in parenthesis, 10 and 50m above sea bed. RunR900 to RunR500 describe different radius of a low pressure disturbance of -60hPa following the trajectory of Run_track2, as described in Table 2.*

3.4 Approximation of functions

Both Section 3.2 and 3.3 involve varying the sea level pressure gradient. A representative value of the pressure gradient for the different scenarios is the dimensionless number $G_{norm}=\frac{P/R}{P_S/R_S}$, where P and R is the actual strength and radius of the low pressure disturbance, while P_S and R_S are values from the standard run, -60hPa and 1000km respectively. By approximating functions which relates maximum current velocities at the different locations OL1 to OL5 at 10 and 50m above seabed to the G_{norm}-values of the different scenarios, it is possible to interpolate and extrapolate maximum velocities to

10 m	OL1	OL2	OL3	OL4	OL5
C_0	0.13457	0.09340	0.03158	0.05232	0.03599
C_1	0.05623	0.11599	0.04163	-0.02789	0.07470
C_2	0.19153	0.09706	0.06968	0.07245	0.04814
max$\|\epsilon\|$	0.02860	0.04666	0.03940	0.01590	0.04660
std.	0.00375	0.00492	0.00411	0.00154	0.00504
50 m					
C_0	0.13595	0.14405	0.04829	0.05225	0.04800
C_1	0.08779	0.11043	0.02777	-0.04866	0.10158
C_0	0.24869	0.13977	0.10129	0.09712	0.05344
max$\|\epsilon\|$	0.03730	0.06069	0.04407	0.02305	0.06520
std.	0.00582	0.00639	0.00418	0.00242	0.00673

Table 7: *Coefficients in a quadratic function approximation (order two) of maximum velocity as a function of normalised pressure gradient, G_{norm}, at OL1 to OL5 at 10 and 50m above seabed. Maximum deviation and standard deviation is also included.*

varying G_{norm}'s.

A set of linearly independent functions, ϕ_k $(k = 0, 1, 2, ..., K)$, is chosen so that the datasets can be estimated as follows:

$$f^* = \sum_{k=0}^{K} c_k \phi_k, \tag{6}$$

where f* is the estimated function of the dataset f giving maximum velocities and c_k is a set of weights which satisfy the so-called normal equations (Dahlquist & Björck 1974):

$$\sum_{k=0} K(\phi_k, \phi_j) c_k = (f, \phi_j), \quad (j = 0, 1, 2, ..., n), \tag{7}$$

where the inner products, ϕ_k, ϕ_j, are scalar products of the vectors. The functions ϕ_k are chosen to be quadratic of order two, corresponding to the equation $f = c_0 + c_1 G_{norm} + c_2 G_{norm}^2$. The normal equations give a matrix to

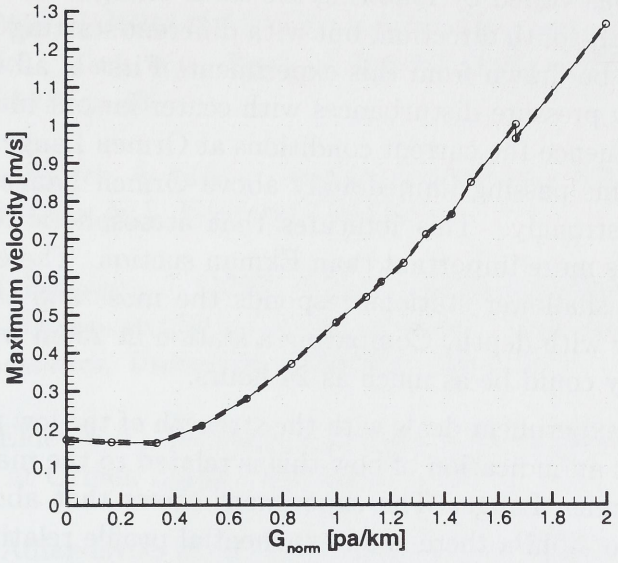

Figure 11: *Maximum velocity (m/s) at OL2, 50m above seabed, as a function of sea level pressure gradient (hPa/km) with model results marked with circles and dashed lines indicating the approximated function.*

solve for each station at both 10 and 50m above seabed. The results of the least square approximation problem including maximum deviation from the real function and the standard deviation is summarised in Table 7. Figure 11 show the approximated function of how maximum velocity at OL2, 50m above seabed, vary with G_{norm}. Above a certain threshold the relation seem close to linear.

4 Final remarks and future work

The numerical studies presented here are an attempt to study how different trajectories, strength of low pressure disturbances and radius of such disturbances affect the maximum current velocities close to the seabed at the shelf slope near Ormen Lange. The model area covers the entire Norwegian Sea basin and the grid size is therefore coarse, 20x20km. The impact of low pressure disturbances on the flow at Ormen Lange is complex and includes processes ranging from large scale to small scale. Although the grid here is coarse the model should nevertheless indicate how the natural system would respond to such an impact.

In the first experiment the distance from the low pressure disturbance to Ormen Lange was varied by following the same straight line with the same angle to the north-south direction, but with different starting points. Several conclusions can be drawn from this experiment. First of all the experiment showed that low pressure disturbances with center far out in the Nordic Sea significantly influence the current conditions at Ormen Lange. Also, it is not necessarily storms passing immediately above Ormen Lange that influence the flow most strongly. This indicates that atmospheric forcing through frictional drag is more important than Ekman suction. The experiment also shows that the shallower stations responds the most and that there is an increasing delay with depth. Comparing a station at 250m with a station at 1100m the delay could be as much as 24 hours.

The second experiment deals with the strength of the low pressure disturbance and gives an indication of how this is related to the maximum current velocities at Ormen Lange. The experiment shows that above a threshold of around -20 to -30hPa there is an exponential profile relating the pressure strength to the maximum velocities, at least at the shallowest stations. This is plausible since the wind stress contains quadratic wind velocity components. The results indicate that the strength of the low pressure disturbance may be more important then the distance from Ormen Lange.

The final experiment investigate the dependence on the radius of the low pressure disturbance and shows that there is an exponential relation between radius and maximum current velocity at Ormen Lange with the largest slopes for the shallowest stations. The results indicate that the radius of the low pressure disturbance strongly affects the maximum current velocity close to the seabed.

Approximation of functions relating maximum velocities at different locations to sea level pressure gradients has been done in the present work. A similar work for measured current velocities and sea level pressure gradients would be of great interest. Obviously, one have to take into account the local topography. Representative stations where the bottom is not too rough should be chosen, and an additional study of how escarpments and local sea mounts would affect the functions is necessary.

Acknowledgements

This work has received support from the Research Council of Norway (Programme for Supercomputing) through a grant of computing time. This work has been supported by Norsk Hydro grant NHT-B44-5098606-00.

References

Berntsen, J. (2000), 'USERS GUIDE for a modesplit σ-coordinate numerical ocean model.', *Tech. rep., Dept. of Applied Mathematics, University of Bergen, Vol.135* p. 48.

Dahlquist, G. & Bjórck, Å. (1974), *Numerical Methods.*, Prentice-Hall, Inc., Englewood Cliffs, N.J. ISBN-0-13-627315-7.

Eliassen, I. K. & Berntsen, J. (2000), 'Using a sigma-coordinate ocean model for simulating the circulation at ormen lange', *Tech. rep., Dept. of Applied Mathematics, University of Bergen, 138* p. 90.

Eliassen, I. K., Eldevik, T., Berntsen, J. & Furnes, G. K. (2000), 'The current conditions at Ormen Lange - Storegga', p. 22.

Engedahl, H., Ådlandsvik, B. & Martinsen, E. A. (1998), 'Production of monthly mean climatological archives of salinity, temperature, current and sea level for the Nordic Seas', *J. Mar. Syst. 14* pp. 1–26.

Engedahl, H. B. & Røed, L. P. (1999), 'Forecasting ocean currents in deep water areas: the Ormen Lange case', *DNMI Reseach Report No. 80, Norwegian Meteorological Institute* .

Gill, A. E. (1982), *Atmosphere-Ocean Dynamics*, Academic Press, Inc. ISBN-0-12-283520-4.

Gjevik, B. (1991), 'Simulations of shelf sea response due to travelling storms.', *Continental Shelf Research, Vol.11, No.2* pp. 139–166.

Hopkins, T. S. (1991), 'The GIN Sea - A synthesis of its physical oceanography and literature review 1972-1985', *Earth-Science Reviews, vol. 30* pp. 175–318.

Lynch, D. R., Ip, J. T. C., Naimie, C. E. & Werner, F. E. (1995), Convergence studies of tidally-rectified circulation on Georges Bank, *in* D. Lynch & A. Davies, eds, 'Quantitative Skill Assessment for Coastal Ocean Models', American Geophysical Union.

Martinsen, E. A. & Engedahl, H. (1987), 'Implementation and testing of a lateral boundary scheme as an open boundary condition in a barotropic ocean model', *Coastal Engineering, Vol.11* pp. 603–627.

Martinsen, E. A., Gjevik, B. & Røed, L. P. (1979), 'A numerical model for long barotropic waves and storm surges along the western coast of Norway', *J.Phys.Oceanogr., Vol.9* pp. 1126–1138.

Mathisen, J. P., Hackett, B. & Engerdahl, H. (2000), 'Description of special current events using observed and simulated data', *OCEANOR report OCN R-99022* .

Stigebrandt, A. (1980), Barotropic and baroclinic response of a semi-enclosed basin to barotropic forcing of the sea, *in* H. J. Freeland, D. M. Farmer & C. D. Levings, eds, 'Proceeding of the NATO Conference on Fjord Oceanography', Plenum Press, New York.

Vikebø, F. B., Berntsen, J. & Furnes, G. K. (2001), 'Analysis of measurements at Ormen Lange', *Tech. rep., Dept. of Applied Mathematics, University of Bergen.* .